

Unit Ball Model for Embedding Hierarchical Structures in the Complex Hyperbolic Space

HUIRU XIAO, Hong Kong University of Science and Technology, Hong Kong SAR, China

CAIGAO JIANG, Ant Group, China

YANGQIU SONG, Hong Kong University of Science and Technology, Hong Kong SAR, China

JAMES ZHANG, Ant Group, China

JUNWU XIONG, Ant Group, China

Learning the representation of data with hierarchical structures in the hyperbolic space attracts increasing attention in recent years. Due to the constant negative curvature, the hyperbolic space resembles tree metrics and captures the tree-like properties naturally, which enables the hyperbolic embeddings to improve over traditional Euclidean models. However, many real-world hierarchically structured data such as taxonomies and multitree networks have varying local structures and they are not trees, thus they do not ubiquitously match the constant curvature property of the hyperbolic space. To address this limitation of hyperbolic embeddings, we explore the complex hyperbolic space, which has the variable negative curvature, for representation learning. Specifically, we propose to learn the embeddings of hierarchically structured data in the unit ball model of the complex hyperbolic space. The unit ball model based embeddings have a more powerful representation capacity to capture a variety of hierarchical structures. Through experiments on synthetic and real-world data, we show that our approach improves over the hyperbolic embedding models significantly. We also explore the competence of complex hyperbolic geometry on the multitree structure and 1- N structure. Our codes are available at <https://github.com/HKUST-KnowComp/UnitBall>.

1 INTRODUCTION

Representation learning of data with hierarchical structures is an important machine learning task with many applications, such as taxonomy induction [14] and hypernymy detection [36]. In recent years, the hyperbolic embeddings [29, 30] have been proposed to improve the traditional Euclidean embedding models. The constant negative curvature of the hyperbolic space produces a manifestation that the hyperbolic space can be regarded as a continuous approximation to trees [24]. The hyperbolic space is capable of embedding any finite tree while preserving the distances approximately [19].

However, most real-world hierarchical data do not belong to tree structures since they can have varying local structures while being tree-like globally. For example, the taxonomies such as WordNet [27] and YAGO [39] contain many 1- N (1 child links to multiple parents) cases and multitree structures [18], which are much more complicated than the tree structure. In consequence, the hyperbolic space which resembles tree metrics has limitations on capturing the general hierarchically structured data.

To address the challenge, in this paper, we propose a new approach to learning the embeddings of hierarchically structured data. Specifically, we embed the hierarchical data into the unit ball model of the complex hyperbolic space. The unit ball model is a projective geometry based model to identify the complex hyperbolic space. One of the main differences between the complex and the real hyperbolic space is that the curvature is non-constant in the complex hyperbolic space. In practice, the variable negative curvature makes the complex hyperbolic space more flexible in handling varying structures while the tree-like properties are still retained.

For empirical evaluation, we evaluate different geometrical embedding models on various hierarchically structured data, including synthetic graphs and real-world data. The experimental results demonstrate the advantages of our approach. In addition, we investigate two specific structures

in which complex hyperbolic geometry shows outstanding performances, namely the multitree structure and 1- N structure, which are highly common and typical in real-world data.

To summarize, our work has the following main contributions:

- (1) We present a novel embedding approach based on the complex hyperbolic geometry to handle data with complicated and various hierarchical structures. To the best of our knowledge, our work is the first to propose complex hyperbolic embeddings.
- (2) We introduce the embedding algorithm in the unit ball model of the complex hyperbolic space. We formulate the learning and Riemannian optimization in the unit ball model.
- (3) We evaluate our approach with experiments on an extensive range of synthetic and real-world data and show the remarkable improvements of our approach.

2 RELATED WORK

Hyperbolic embeddings. Hyperbolic embedding methods have become the leading approach for representation learning of hierarchical structures. Nickel and Kiela [29] learned the representations of hierarchical graphs in the Poincaré ball model of the hyperbolic space and outperformed the Euclidean embedding methods for taxonomies. The Poincaré embedding model was then improved by follow-up works on hyperbolic embeddings [15, 30]. These methods learned the hyperbolic embeddings by Riemannian optimization [4], which was further improved by the Riemannian adaptive optimization [3].

Another branch of study [33, 38] learned the hyperbolic embeddings through combinatorial construction. Instead of optimizing the soft-ranking loss by Riemannian optimization as in [29, 30], the construction-based methods minimize the reconstruction distortion by combinatorial construction. However, both the optimization-based and construction-based hyperbolic embeddings suffer from the limitation in hierarchical graphs with varying local structures. To tackle the challenge, Gu et al. [20] extended the construction-based method by jointly learning the curvature and the embeddings of data in a product manifold. Although it can provide a better representation than a single space with constant curvature, it is impractical to search for the best manifold combination among enormous combinations for each new structure.

Motivated by the promising results of previous works, extensions to the multi-relational graph hyperbolic embeddings [1, 7, 40] and hyperbolic neural networks [8, 11, 16, 21, 25, 35, 45] were explored. Notably, [7, 8] leverages the trainable curvature to compensate for the disparity between the actual data structures and the constant-curvature hyperbolic space, where each layer in the graph neural network or each relation in the multi-relational graph has its own curvature parameterization. The hyperbolic learning also inspired other research tasks and applications, such as classification [9], image reconstruction [37], text generation [12], etc.

Complex embeddings. The traditional knowledge graph embeddings were learned in the real Euclidean space [5, 31, 44] and were used for knowledge graph inference and reasoning. In recent years, several works suggested utilizing the complex Euclidean space for inferring more relation patterns, such as ComplEx [42] and RotatE [41]. These models have been demonstrated to be effective in knowledge graph embeddings. The success of the complex embeddings reveals the potential of the complex space and inspires us to explore the complex hyperbolic space.

3 PRELIMINARIES

3.1 Basic Definitions

Before introducing the hyperbolic geometry and the complex hyperbolic geometry, we need to explain and define some related concepts. The first one is *curvature*, which describes the curve of Riemannian manifolds and controls the rate of geodesic deviation.¹

3.1.1 Curvature.

DEFINITION 1 (CURVATURE). *Given a Riemannian manifold and two linearly independent tangent vectors at the same point, \mathbf{u} and \mathbf{v} , the **(sectional) curvature** is defined as*

$$K(\mathbf{u}, \mathbf{v}) = \frac{\langle R(\mathbf{u}, \mathbf{v})\mathbf{v}, \mathbf{u} \rangle}{\langle \mathbf{u}, \mathbf{u} \rangle \langle \mathbf{v}, \mathbf{v} \rangle - \langle \mathbf{u}, \mathbf{v} \rangle^2},$$

where R is the Riemann curvature tensor, defined by the convention $R(\mathbf{u}, \mathbf{v})\mathbf{w} = \nabla_{\mathbf{u}}\nabla_{\mathbf{v}}\mathbf{w} - \nabla_{\mathbf{v}}\nabla_{\mathbf{u}}\mathbf{w} - \nabla_{[\mathbf{u}, \mathbf{v}]}\mathbf{w}$. Here ∇ indicates the Levi-Civita connection, whose definitions are given below.

Before defining Levi-Civita connection, we need to first define the affine connection.

DEFINITION 2 (AFFINE CONNECTION). *Let M be a smooth manifold and let $\Gamma(\mathcal{T}M)$ be the space of vector fields on M , i.e., the space of smooth sections of the tangent bundle $\mathcal{T}M$. Then an **affine connection** on M is a bilinear map*

$$\begin{aligned} \Gamma(\mathcal{T}M) \times \Gamma(\mathcal{T}M) &\rightarrow \Gamma(\mathcal{T}M) \\ (X, Y) &\mapsto \nabla_X Y, \end{aligned}$$

such that for all f in the set of smooth functions on M , written $C^\infty(M, \mathbb{R})$, and all vector fields X, Y on M :

- (1) $\nabla_{fX}Y = f\nabla_XY$, i.e., ∇ is $C^\infty(M, \mathbb{R})$ -linear in the first variable;
- (2) $\nabla_X(fY) = \partial_X fY + f\nabla_XY$, where ∂_X denotes the directional derivative, i.e., ∇ satisfies Leibniz rule in the second variable.

Next, we define the Levi-Civita connection.

DEFINITION 3 (LEVI-CIVITA CONNECTION). *An affine connection ∇ is called a **Levi-Civita connection** if*

- (1) it preserves the metric, i.e., $\nabla g = 0$.
- (2) it is torsion-free, i.e., for any vector fields X and Y we have $\nabla_XY - \nabla_YX = [X, Y]$, where $[X, Y]$ is the Lie bracket of the vector fields X and Y .

3.1.2 δ -Hyperbolicity. Here we give the definition of δ -hyperbolicity [19], which measures the tree-likeness of graphs. The lower δ corresponds to the more tree-like graph. Trees have 0 δ -hyperbolicity.

DEFINITION 4 (δ -HYPERBOLICITY). *Let a, b, c, d be vertices of the graph G . Let S_1, S_2 and S_3 be*

$$S_1 = \text{dist}(a, b) + \text{dist}(d, c), S_2 = \text{dist}(a, c) + \text{dist}(b, d), S_3 = \text{dist}(a, d) + \text{dist}(b, c).$$

Suppose M_1 and M_2 are the two largest values among S_1, S_2, S_3 and $M_1 \geq M_2$. Define $\text{hyp}(a, b, c, d) = M_1 - M_2$. Then the **δ -hyperbolicity** of G is defined as

$$\delta(G) = \frac{1}{2} \max_{a, b, c, d \in V(G)} \text{hyp}(a, b, c, d).$$

That is, $\delta(G)$ is the maximum of hyp over all possible 4-tuples (a, b, c, d) divided by 2.

¹In this paper, curvature refers to the sectional curvature.

3.2 Hyperbolic Geometry

Hyperbolic space² is a homogeneous space with constant negative curvature. In the hyperbolic space $\mathbb{H}_{\mathbb{R}}^n(K)$ of dimension n and curvature K , the volume of a ball grows exponentially with its radius ρ :

$$\text{vol}(B_{\mathbb{H}_{\mathbb{R}}^n(K)}(\rho)) \sim e^{\sqrt{-K}(n-1)\rho}. \quad (1)$$

Contrastively, in the Euclidean space \mathbb{E}^n , the curvature is 0 and the volume of a ball grows polynomially with its radius:

$$\text{vol}(B_{\mathbb{E}^n}(\rho)) = \frac{\pi^{n/2}}{\Gamma(n/2)} \rho^n \sim \rho^n. \quad (2)$$

The exponential volume growth rate enables the hyperbolic space to have powerful representation capability for tree structures since the number of nodes grows exponentially with the depth in a tree, while the Euclidean space is too flat and narrow to embed trees.

3.3 Complex Hyperbolic Geometry

Complex hyperbolic space is a homogeneous space of variable negative curvature. Its ambient Hermitian vector space $\mathbb{C}^{n,1}$ is the complex Euclidean space \mathbb{C}^{n+1} endowed with some Hermitian form $\langle\langle \mathbf{z}, \mathbf{w} \rangle\rangle$, where $\mathbf{z}, \mathbf{w} \in \mathbb{C}^{n+1}$. Then the Hermitian space $\mathbb{C}^{n,1}$ can be divided into three subsets: $V_- = \{\mathbf{z} \in \mathbb{C}^{n,1} | \langle\langle \mathbf{z}, \mathbf{z} \rangle\rangle < 0\}$, $V_0 = \{\mathbf{z} \in \mathbb{C}^{n,1} - \{0\} | \langle\langle \mathbf{z}, \mathbf{z} \rangle\rangle = 0\}$, and $V_+ = \{\mathbf{z} \in \mathbb{C}^{n,1} | \langle\langle \mathbf{z}, \mathbf{z} \rangle\rangle > 0\}$. Let \mathbb{P} be a projection map $\mathbb{P} : \mathbb{C}^{n,1} - \{z_{n+1} = 0\} \rightarrow \mathbb{C}^n$, i.e.,

$$\mathbb{P} : \begin{bmatrix} z_1 \\ \vdots \\ z_{n+1} \end{bmatrix} \mapsto \begin{bmatrix} z_1/z_{n+1} \\ \vdots \\ z_n/z_{n+1} \end{bmatrix}, \text{ where } z_{n+1} \neq 0. \quad (3)$$

Then the complex hyperbolic space $\mathbb{H}_{\mathbb{C}}^n$ and its boundary $\partial\mathbb{H}_{\mathbb{C}}^n$ are defined using the projectivization:

$$\mathbb{H}_{\mathbb{C}}^n = \mathbb{P}V_-, \quad \partial\mathbb{H}_{\mathbb{C}}^n = \mathbb{P}V_0. \quad (4)$$

3.3.1 The Unit Ball Model. The unit ball model is one model used to identify the complex hyperbolic space, which can be derived via the projective geometry [17]. We now provide the necessary derivation.

Take the abovementioned Hermitian form of $\mathbb{C}^{n,1}$ to be a standard Hermitian form:

$$\langle\langle \mathbf{z}, \mathbf{w} \rangle\rangle = z_1 \bar{w}_1 + \cdots + z_n \bar{w}_n - z_{n+1} \bar{w}_{n+1}, \quad (5)$$

where \bar{w} is the conjugate of w . Take $z_{n+1} = 1$ in the projection map \mathbb{P} in Eq. (3). Then from Eq. (4), we can derive the formula of the unit ball model:

$$\mathcal{B}_{\mathbb{C}}^n = \mathbb{P}(\{\mathbf{z} \in \mathbb{C}^{n,1} | \langle\langle \mathbf{z}, \mathbf{z} \rangle\rangle < 0\}) = \{(z_1, \dots, z_n, 1) | |z_1|^2 + \cdots + |z_n|^2 < 1\}. \quad (6)$$

The metric on $\mathcal{B}_{\mathbb{C}}^n$ is Bergman metric, which takes the formula below in 2-d case:

$$ds^2 = \frac{-4}{\langle\langle \mathbf{z}, \mathbf{z} \rangle\rangle^2} \det \begin{bmatrix} \langle\langle \mathbf{z}, \mathbf{z} \rangle\rangle & \langle\langle d\mathbf{z}, \mathbf{z} \rangle\rangle \\ \langle\langle \mathbf{z}, d\mathbf{z} \rangle\rangle & \langle\langle d\mathbf{z}, d\mathbf{z} \rangle\rangle \end{bmatrix}. \quad (7)$$

The distance function on $\mathcal{B}_{\mathbb{C}}^n$ is given by

$$d_{\mathcal{B}_{\mathbb{C}}^n}(\mathbf{z}, \mathbf{w}) = \text{arcosh} \left(2 \frac{\langle\langle \mathbf{z}, \mathbf{w} \rangle\rangle \langle\langle \mathbf{w}, \mathbf{z} \rangle\rangle}{\langle\langle \mathbf{z}, \mathbf{z} \rangle\rangle \langle\langle \mathbf{w}, \mathbf{w} \rangle\rangle} - 1 \right), \quad (8)$$

²In this paper, we use *hyperbolic space* to refer to real hyperbolic space and *hyperbolic embeddings* to refer to real hyperbolic embeddings for avoiding wordiness.

The distance function maintains the tree-like metric properties. When the points are very close to the origin, it approximates to the Euclidean distance. Additionally, when a point is closer to the origin, it has relatively smaller distances to the other points. Correspondingly, the points near the boundary have very large distances from each other. Therefore, in ideal conditions, the root node of a tree is embedded in the origin while the deeper nodes are embedded farther away from the origin. Recall that the distance function in the real hyperbolic space [29] has similar properties since the real hyperbolic space, as the totally geodesic subspace of the complex hyperbolic space, inherits the tree-like metrics. More details about the Bergman metric and distance function can be referred to Chapter 3.1 in [17].

Note that there are other choices of the Hermitian form $\langle\langle \mathbf{z}, \mathbf{w} \rangle\rangle$, which corresponds to other models of complex hyperbolic geometry, such as the Siegel domain model. We choose the unit ball model for the relatively simple formula as well as convenient computations of the metric and distance function.

3.3.2 Variable Negative Curvature. The curvature of the complex hyperbolic space is summarized by [17] as follows:

THEOREM 1. *The curvature is not constant in $\mathbb{H}_{\mathbb{C}}^n$. It is pinched between -1 (in the directions of complex projective lines) and $-1/4$ (in the directions of totally real planes).*

Before proving Theorem 1, we need to introduce the definition of *Kähler structure* [28].

DEFINITION 5 (KÄHLER STRUCTURE). *A **Kähler structure** can be defined in any of the following equivalent ways:*

- (1) *A complex structure with a closed, positive $(1, 1)$ -form.*
- (2) *A Riemannian structure with a complex structure such that the corresponding exterior 2-form is closed.*
- (3) *A symplectic structure with a compatible integrable almost complex structure which is positive.*

Recall that the complex hyperbolic space $\mathbb{H}_{\mathbb{C}}^n$ is defined using the projectivization of the negative zone with a Hermitian form $\langle\langle \mathbf{z}, \mathbf{w} \rangle\rangle$. Denote ω as the imaginary part of the Hermitian form $\langle\langle \cdot, \cdot \rangle\rangle$, i.e., $\omega(\mathbf{z}, \mathbf{w}) = \frac{1}{2i}(\langle\langle \mathbf{z}, \mathbf{w} \rangle\rangle - \langle\langle \mathbf{w}, \mathbf{z} \rangle\rangle)$, then according to [17], the metric ω is *positive* and *closed*, and necessarily has type $(1, 1)$. Then by the first definition in Definition 5, $\mathbb{H}_{\mathbb{C}}^n$ is a Kähler structure.

Let M be a Kähler manifold and $\mathbf{z} \in M$. Denote $\mathcal{T}_{\mathbf{z}}M$ as the tangent space of M at \mathbf{z} and $J : \mathcal{T}M \rightarrow \mathcal{T}M$ is an endomorphism. As proved in [23], the curvature of real 2-planes in the tangent space $\mathcal{T}_{\mathbf{z}}M$ has the following properties:

THEOREM 2. *Let M be a connected Kähler manifold of complex dimension $n \geq 2$. If the holomorphic sectional curvature $K(p)$, where p is a plane in $\mathcal{T}_{\mathbf{z}}M$ invariant by J , depends only on \mathbf{z} , then M is a space of constant holomorphic sectional curvature.*

Next, we give a proposition in [23], which is about the curvature of a plane.

PROPOSITION 1. *If \mathbf{u}, \mathbf{v} is an orthonormal basis for a plane p and if we set the curvature of p as $K(p) = R(\mathbf{u}, \mathbf{v})$, where $R(\mathbf{u}, \mathbf{v})$ is the Riemann curvature tensor, then*

$$K(p) = \frac{1}{4}(1 + 3 \cos^2 \alpha(p)),$$

where $\alpha(p)$ is the angle between p and $J(p)$.

Finally, we prove Theorem 1 as follows.

PROOF. Let M be a Kähler manifold and $z \in M$. From Theorem 2, the corresponding sectional curvature function of real 2-planes in $\mathcal{T}_z M$ is completely determined by the sectional curvature function restricted to complex lines in $\mathcal{T}_z M$. If the sectional curvature of every complex line in $\mathcal{T}M$ equals κ , then M is said to have constant holomorphic sectional curvature κ .

Then from Proposition 1, we can know that in this case, the sectional curvature of a 2-dimensional subspace $S \subset \mathcal{T}M$ is

$$K(S) = \kappa \frac{1 + 3 \cos^2 \alpha(S)}{4}, \quad (9)$$

where $\alpha(S)$ is the angle of holomorphy, defined as the smallest angle between two nonzero vectors from two linear subspaces of the underlying real vector space of M .

In particular, the complex hyperbolic space $\mathbb{H}_{\mathbb{C}}^n$ is a Kähler structure with $\kappa = -1$. Since $0 \leq \cos^2 \alpha(S) \leq 1$, then from Eq. (9), we can have $-1 \leq K(S) \leq -1/4$ for any 2-dimensional subspace $S \subset \mathcal{T}M$ of $\mathbb{H}_{\mathbb{C}}^n$, i.e., the (sectional) curvature is not constant in $\mathbb{H}_{\mathbb{C}}^n$, but pinched between -1 and $-1/4$. Thus we proved the non-constant curvature of $\mathbb{H}_{\mathbb{C}}^n$.

Specifically, we discuss the complex projective lines and totally real planes in the unit ball model of the complex hyperbolic space: $\mathcal{B}_{\mathbb{C}}^n = \{(z_1, \dots, z_n, 1) \mid |z_1|^2 + \dots + |z_n|^2 < 1\}$.

First let's consider the case of complex projective lines. Consider a complex line L in \mathbb{C}^n that intersects the unit ball model $\mathcal{B}_{\mathbb{C}}^n$. Let z be any point in $L \cap \mathcal{B}_{\mathbb{C}}^n$. We can apply an element of $\text{PU}(n, 1)$ to L so that it becomes the last coordinate axis $\{(0, z_n) \mid z_n \in \mathbb{C}\}$, whose intersection with $\mathcal{B}_{\mathbb{C}}^n$ is the disk $|z_n| < 1$. Then the restriction of the Bergman metric to this disc is the Poincaré metric [2] of constant curvature -1 .

In order to see this, let $z = (0, z_n, 1)$ and $w = (0, w_n, 1)$, $z, w \in L \cap \mathcal{B}_{\mathbb{C}}^n$, then from Eq. (9) in Section 3.3.1, the distance between z and w is given by Eq. (8). Then we have

$$\cosh^2\left(\frac{d_{\mathcal{B}_{\mathbb{C}}^n}(z, w)}{2}\right) = \frac{\langle\langle z, w \rangle\rangle \langle\langle w, z \rangle\rangle}{\langle\langle z, z \rangle\rangle \langle\langle w, w \rangle\rangle} = \frac{|z_n \overline{w_n} - 1|^2}{(|z_n|^2 - 1)(|w_n|^2 - 1)}, \quad (10)$$

which is just the Poincaré metric [2].

Next consider a totally real plane p . Any totally real plane p is the image under an element of $\text{PU}(n, 1)$ of the subspace comprising those points of $\mathcal{B}_{\mathbb{C}}^n$ with real coordinates, that is actually an embedded copy of the real hyperbolic space $\mathbb{H}_{\mathbb{R}}^n = \{(x_1, \dots, x_n) \mid x_1, \dots, x_n \in \mathbb{R}\}$. This subspace intersects $\mathcal{B}_{\mathbb{C}}^n$ in the subset consisting of those points with $x_1^2 + \dots + x_n^2 < 1$. Then the Bergman metric restricted to this real-space unit ball is just the Klein-Beltrami metric [32] on the unit ball in \mathbb{R}^n with constant curvature $-1/4$.

To see this, let $x = (x_1, \dots, x_n, 1)$ and $y = (y_1, \dots, y_n, 1)$, $x, y \in \mathbb{H}_{\mathbb{R}}^n \cap \mathcal{B}_{\mathbb{C}}^n$, then apply the similar process with the above, we have

$$\cosh^2\left(\frac{d_{\mathcal{B}_{\mathbb{C}}^n}(x, y)}{2}\right) = \frac{\langle\langle x, y \rangle\rangle \langle\langle y, x \rangle\rangle}{\langle\langle x, x \rangle\rangle \langle\langle y, y \rangle\rangle} = \frac{(x_1 y_1 + \dots + x_n y_n - 1)^2}{(x_1^2 + \dots + x_n^2 - 1)(y_1^2 + \dots + y_n^2 - 1)}, \quad (11)$$

which is the Klein-Beltrami metric [32] on the unit ball in \mathbb{R}^n with constant curvature $-1/4$.

Therefore, we proved that the curvature of $\mathbb{H}_{\mathbb{C}}^n$ is -1 in the directions of complex projective lines while $-1/4$ in the directions of totally real planes. \square

REMARK. *Curvature in the complex hyperbolic space is a very complicated topic in geometric group theory and differential geometry. The complex projective lines and the totally real planes are two kinds of special subspaces, whose curvatures are presented above. For the subspace that lives in between the two special cases, we refer the interested readers to [13] for an interesting example in the complex hyperbolic space (its curvature differs with our work with a constant multiplier 4). In Section 5 and*

Table 1. Comparison of Euclidean, hyperbolic, and complex hyperbolic geometries. n denotes the dimensionality and ρ denotes the radius of the ball.

Geometry	Curvature	Volume growth of ball
Euclidean	0 (constant)	$\sim \rho^n$ (polynomially)
Hyperbolic	$K < 0$ (constant negative)	$\sim e^{\sqrt{-K}(n-1)\rho}$ (exponentially)
Complex hyperbolic	pinched between -1 and $-\frac{1}{4}$ (variable negative)	$\sim e^{n\rho}$ (exponentially)

Figure 5 of [13], the author explored the curvature of a triangle in complex hyperbolic geometry with numerical computation.

The non-constant curvature, which we expect to be favorable for embedding various hierarchical structures, is one of the main differences between $\mathbb{H}_{\mathbb{C}}^n$ and $\mathbb{H}_{\mathbb{R}}^n$.

3.3.3 Exponential Volume Growth. The complex hyperbolic space also has the tree-like exponential volume growth property. The volume of a ball with radius ρ in $\mathbb{H}_{\mathbb{C}}^n$ is given by

$$\text{vol}(B_{\mathbb{H}_{\mathbb{C}}^n}(\rho)) = \frac{8^n \sigma_{2n-1}}{2n} \sinh^{2n}(\rho/2) \sim e^{n\rho}, \quad (12)$$

where $\sigma_{2n-1} = 2\pi^n/n!$ is the Euclidean volume of the unit sphere $S^{2n-1} \in \mathbb{C}^n$.

From the properties of the complex hyperbolic geometry, we expect that the complex hyperbolic space can naturally handle data with diverse local structures in virtue of the variable curvature as presented in Theorem 1 while preserving the tree-like properties as shown in Eq. (12). In summary, Table 1 outlines our concerned properties of Euclidean, hyperbolic, and complex hyperbolic geometry.

From this section, we see that complex hyperbolic geometry and hyperbolic geometry are typically of different characteristics. The n -dimensional (n -d) complex hyperbolic space is not simply the $2n$ -d hyperbolic space or the product of two n -d hyperbolic spaces. This implies that our complex hyperbolic embedding model is intrinsically different from the hyperbolic embedding methods [29, 30] or the product manifold embeddings [20].

4 UNIT BALL EMBEDDINGS

We propose to embed the hierarchically structured data into the unit ball model of the complex hyperbolic space. In this section, we introduce our approach in detail.

4.1 Embeddings in the Unit Ball Model

Given the hierarchical data containing a set of nodes $X = \{x_p\}_{p=1}^m$ and a set of edges $E = \{(x_p, x_q) | x_p, x_q \in X\}$, we aim to learn the embeddings of the nodes $Z = \{z_p\}_{p=1}^m$, where $z_p \in \mathcal{B}_{\mathbb{C}}^n = \{(z_1, \dots, z_n, 1) | |z_1|^2 + \dots + |z_n|^2 < 1\}$ (Eq. (6)).

The objective of the embeddings is to recover the structures of input data, including the distances between the nodes as well as the partial order in the hierarchies. Here we adopt the soft ranking loss used in the Poincaré ball embeddings [29] and the hyperboloid embeddings [30], which aims at preserving the hierarchical relationships among nodes:

$$L = \sum_{(x_p, x_q) \in E} \log \frac{e^{-d_{\mathcal{B}_{\mathbb{C}}^n}(z_p, z_q)}}{\sum_{x_k \in \mathcal{N}(x_p)} e^{-d_{\mathcal{B}_{\mathbb{C}}^n}(z_p, z_k)}}, \quad (13)$$

Algorithm 1 RSGD of the unit ball embeddings.

Input: initialization $\mathbf{z}^{(0)}$, number of iterations T , learning rates $\{\eta^{(t)}\}_{t=1}^T$.
for $t = 1$ **to** T **do**
 Compute $\frac{\partial d_{\mathcal{B}_{\mathbb{C}}^n}}{\partial \mathbf{x}}$ and $\frac{\partial d_{\mathcal{B}_{\mathbb{C}}^n}}{\partial \mathbf{y}}$ by Eqs. (22) and (23).
 Compute $\nabla_E L(\mathbf{z})$ and $\nabla_R L(\mathbf{z})$ by Eq. (15).
 Update $\mathbf{z}^{(t)}$ by Eq. (25).
end for

where $\mathcal{N}(x_p) = \{x_k : (x_p, x_k) \notin E\} \cup \{x_p\}$ is the set of negative examples for x_p together with x_p . $d_{\mathcal{B}_{\mathbb{C}}^n}$ is the distance function in the unit ball model given in Eq. (8). The minimization of L makes the connected nodes closer in the embedding space than those with no observed edges.

The learning process implicitly aligns the geometric structures of the embedding space and the underlying graph structures of data since the loss function aims at preserving the hierarchical relationships among nodes while the underlying graph structures are reflected by the hierarchical relationships. We learn the embeddings in the unit ball model, where the variable negative curvature of the complex hyperbolic space provides the capacity to deal with more varying structures. The experiments in Section 5 exhibit that the unit ball model learns the high-quality embeddings and captures the various hierarchical structures.

4.2 Riemannian Optimization in the Unit Ball Model

We learn the embeddings $\mathbf{Z} = \{\mathbf{z}_p\}_{p=1}^m$ through solving the optimization problem with constraint:

$$\mathbf{Z} \leftarrow \arg \min_{\mathbf{Z}} L \quad \text{s.t. } \forall \mathbf{z}_p \in \mathbf{Z}, \mathbf{z}_p \in \mathcal{B}_{\mathbb{C}}^n. \quad (14)$$

For the optimization problems in Riemannian manifolds, Bonnabel [4] presented the Riemannian stochastic gradient descent (RSGD) algorithm, which we employ to optimize Eq. (14). To update an embedding $\mathbf{z} \in \mathcal{B}_{\mathbb{C}}^n$,³ we need to obtain its Riemannian gradient ∇_R . Specifically, the embedding is updated at the t -th iteration by $\mathbf{z}^{(t)} \leftarrow \mathbf{z}^{(t-1)} - \eta^{(t)} \nabla_R L(\mathbf{z})$, where $\eta^{(t)}$ is the learning rate at the t -th iteration and $\nabla_R L(\mathbf{z})$ is the Riemannian gradient of $L(\mathbf{z})$.

The Riemannian gradient ∇_R can be derived from rescaling the Euclidean gradient ∇_E with the inverse of the metric tensor ds^2 in Eq. (7). Apply the chain rule of differential functions and we have:

$$\nabla_R L(\mathbf{z}) = \frac{1}{ds^2} \nabla_E L(\mathbf{z}) = \frac{1}{ds^2} \frac{\partial L(\mathbf{z})}{\partial d_{\mathcal{B}_{\mathbb{C}}^n}(\mathbf{z}, \mathbf{w})} \nabla_E d_{\mathcal{B}_{\mathbb{C}}^n}(\mathbf{z}, \mathbf{w}). \quad (15)$$

$\frac{\partial L(\mathbf{z})}{\partial d_{\mathcal{B}_{\mathbb{C}}^n}(\mathbf{z}, \mathbf{w})}$ is trivial to compute from Eq. (13). In practical training, we implement and compute the complex hyperbolic embedding as its real part and imaginary part, i.e., $\mathbf{z} = \mathbf{x} + i\mathbf{y}$, where i represents the *imaginary unit*, i.e., $i^2 = -1$. In order to get the gradient of the distance function $\nabla_E d_{\mathcal{B}_{\mathbb{C}}^n}(\mathbf{z}, \mathbf{w})$ in Eq. (15), we get the partial derivative with regard to the real part and the imaginary part, i.e., $\nabla_E d_{\mathcal{B}_{\mathbb{C}}^n}(\mathbf{z}, \mathbf{w}) = \frac{\partial d_{\mathcal{B}_{\mathbb{C}}^n}(\mathbf{z}, \mathbf{w})}{\partial \mathbf{x}} + i \frac{\partial d_{\mathcal{B}_{\mathbb{C}}^n}(\mathbf{z}, \mathbf{w})}{\partial \mathbf{y}}$. The distance function in the unit ball model is given by Eq. (8). The full derivation of $\frac{\partial d_{\mathcal{B}_{\mathbb{C}}^n}(\mathbf{z}, \mathbf{w})}{\partial \mathbf{x}}$ and $\frac{\partial d_{\mathcal{B}_{\mathbb{C}}^n}(\mathbf{z}, \mathbf{w})}{\partial \mathbf{y}}$ is as follows.

First, we need to introduce Wirtinger derivatives [43], which constructs a differential calculus for differential functions on complex domains.

³Here we omit the subscript of \mathbf{z}_p for concision.

DEFINITION 6 (WIRTINGER DERIVATIVES). *The partial derivatives of a (complex) function $f(z)$ of a complex variable $z = x + iy \in \mathbb{C}$, $x, y \in \mathbb{R}$, with respect to z and $\bar{z} = x - iy$, respectively, are defined as:*

$$\frac{\partial f(z, \bar{z})}{\partial z} = \frac{1}{2} \left(\frac{\partial}{\partial x} - i \frac{\partial}{\partial y} \right) f(z, \bar{z}), \quad \frac{\partial f(z, \bar{z})}{\partial \bar{z}} = \frac{1}{2} \left(\frac{\partial}{\partial x} + i \frac{\partial}{\partial y} \right) f(z, \bar{z}).$$

The Wirtinger derivatives can be rewritten as:

$$\frac{\partial f(z, \bar{z})}{\partial x} = \left(\frac{\partial}{\partial z} + \frac{\partial}{\partial \bar{z}} \right) f(z, \bar{z}), \quad (16)$$

$$\frac{\partial f(z, \bar{z})}{\partial y} = i \left(\frac{\partial}{\partial z} - \frac{\partial}{\partial \bar{z}} \right) f(z, \bar{z}), \quad (17)$$

Let $p = \cosh(d_{\mathcal{B}_{\mathbb{C}}^n}(\mathbf{z}, \mathbf{w})) = 2 \frac{\langle\langle \mathbf{z}, \mathbf{w} \rangle\rangle \langle\langle \mathbf{w}, \mathbf{z} \rangle\rangle}{\langle\langle \mathbf{z}, \mathbf{z} \rangle\rangle \langle\langle \mathbf{w}, \mathbf{w} \rangle\rangle} - 1$, then $d_{\mathcal{B}_{\mathbb{C}}^n}(\mathbf{z}, \mathbf{w}) = \operatorname{arcosh}(p) = \ln(p + \sqrt{p^2 - 1})$. Let $\mathbf{z} = (z_1, \dots, z_n, 1) \in \mathcal{B}_{\mathbb{C}}^n$, then

$$\begin{aligned} \frac{\partial d_{\mathcal{B}_{\mathbb{C}}^n}(\mathbf{z}, \mathbf{w})}{\partial z_j} &= \frac{\partial d_{\mathcal{B}_{\mathbb{C}}^n}(\mathbf{z}, \mathbf{w})}{\partial p} \cdot \frac{\partial p}{\partial z_j} = \frac{1}{\sqrt{p^2 - 1}} \cdot \frac{\partial p}{\partial z_j} = \frac{2}{\sqrt{p^2 - 1}} \cdot \frac{\partial \frac{(z_1 \bar{w}_1 + \dots + z_n \bar{w}_n - 1) \cdot \langle\langle \mathbf{w}, \mathbf{z} \rangle\rangle}{(z_1 \bar{z}_1 + \dots + z_n \bar{z}_n - 1) \cdot \langle\langle \mathbf{w}, \mathbf{w} \rangle\rangle}}{\partial z_j} \\ &= \frac{2}{\sqrt{p^2 - 1}} \cdot \left(\frac{\bar{w}_j \langle\langle \mathbf{w}, \mathbf{z} \rangle\rangle}{\langle\langle \mathbf{z}, \mathbf{z} \rangle\rangle \cdot \langle\langle \mathbf{w}, \mathbf{w} \rangle\rangle} - \frac{\bar{z}_j \langle\langle \mathbf{z}, \mathbf{w} \rangle\rangle \cdot \langle\langle \mathbf{w}, \mathbf{z} \rangle\rangle}{\langle\langle \mathbf{z}, \mathbf{z} \rangle\rangle^2 \cdot \langle\langle \mathbf{w}, \mathbf{w} \rangle\rangle} \right), \end{aligned} \quad (18)$$

for $1 \leq j \leq n$. Similarly, we can have

$$\frac{\partial d_{\mathcal{B}_{\mathbb{C}}^n}(\mathbf{z}, \mathbf{w})}{\partial \bar{z}_j} = \frac{2}{\sqrt{p^2 - 1}} \cdot \left(\frac{w_j \langle\langle \mathbf{z}, \mathbf{w} \rangle\rangle}{\langle\langle \mathbf{z}, \mathbf{z} \rangle\rangle \cdot \langle\langle \mathbf{w}, \mathbf{w} \rangle\rangle} - \frac{z_j \langle\langle \mathbf{z}, \mathbf{w} \rangle\rangle \cdot \langle\langle \mathbf{w}, \mathbf{z} \rangle\rangle}{\langle\langle \mathbf{z}, \mathbf{z} \rangle\rangle^2 \cdot \langle\langle \mathbf{w}, \mathbf{w} \rangle\rangle} \right). \quad (19)$$

Then by Eqs. (16), (18), and (19), we obtain

$$\frac{\partial d_{\mathcal{B}_{\mathbb{C}}^n}}{\partial x_j} = \frac{\partial d_{\mathcal{B}_{\mathbb{C}}^n}(\mathbf{z}, \mathbf{w})}{\partial z_j} + \frac{\partial d_{\mathcal{B}_{\mathbb{C}}^n}(\mathbf{z}, \mathbf{w})}{\partial \bar{z}_j} = \frac{4}{\sqrt{p^2 - 1}} \left(\frac{\operatorname{Re}(\langle\langle \mathbf{z}, \mathbf{w} \rangle\rangle w_j)}{\langle\langle \mathbf{z}, \mathbf{z} \rangle\rangle \langle\langle \mathbf{w}, \mathbf{w} \rangle\rangle} - \frac{\langle\langle \mathbf{z}, \mathbf{w} \rangle\rangle \langle\langle \mathbf{w}, \mathbf{z} \rangle\rangle x_j}{\langle\langle \mathbf{z}, \mathbf{z} \rangle\rangle^2 \langle\langle \mathbf{w}, \mathbf{w} \rangle\rangle} \right). \quad (20)$$

Similarly, by Eqs. (17), (18), and (19), we can get

$$\frac{\partial d_{\mathcal{B}_{\mathbb{C}}^n}}{\partial y_j} = i \left(\frac{\partial d_{\mathcal{B}_{\mathbb{C}}^n}(\mathbf{z}, \mathbf{w})}{\partial z_j} - \frac{\partial d_{\mathcal{B}_{\mathbb{C}}^n}(\mathbf{z}, \mathbf{w})}{\partial \bar{z}_j} \right) = \frac{4}{\sqrt{p^2 - 1}} \left(\frac{\operatorname{Im}(\langle\langle \mathbf{z}, \mathbf{w} \rangle\rangle w_j)}{\langle\langle \mathbf{z}, \mathbf{z} \rangle\rangle \langle\langle \mathbf{w}, \mathbf{w} \rangle\rangle} - \frac{\langle\langle \mathbf{z}, \mathbf{w} \rangle\rangle \langle\langle \mathbf{w}, \mathbf{z} \rangle\rangle y_j}{\langle\langle \mathbf{z}, \mathbf{z} \rangle\rangle^2 \langle\langle \mathbf{w}, \mathbf{w} \rangle\rangle} \right), \quad (21)$$

where $\operatorname{Re}(\cdot)$ and $\operatorname{Im}(\cdot)$ denote the real and the imaginary part respectively. Then the partial derivatives of the unit ball model distance take the following formulas:

$$\frac{\partial d_{\mathcal{B}_{\mathbb{C}}^n}}{\partial \mathbf{x}} = \frac{4}{\sqrt{p^2 - 1}} \left(\frac{\operatorname{Re}(\langle\langle \mathbf{z}, \mathbf{w} \rangle\rangle \mathbf{w})}{\langle\langle \mathbf{z}, \mathbf{z} \rangle\rangle \langle\langle \mathbf{w}, \mathbf{w} \rangle\rangle} - \frac{\langle\langle \mathbf{z}, \mathbf{w} \rangle\rangle \langle\langle \mathbf{w}, \mathbf{z} \rangle\rangle \mathbf{x}}{\langle\langle \mathbf{z}, \mathbf{z} \rangle\rangle^2 \langle\langle \mathbf{w}, \mathbf{w} \rangle\rangle} \right), \quad (22)$$

$$\frac{\partial d_{\mathcal{B}_{\mathbb{C}}^n}}{\partial \mathbf{y}} = \frac{4}{\sqrt{p^2 - 1}} \left(\frac{\operatorname{Im}(\langle\langle \mathbf{z}, \mathbf{w} \rangle\rangle \mathbf{w})}{\langle\langle \mathbf{z}, \mathbf{z} \rangle\rangle \langle\langle \mathbf{w}, \mathbf{w} \rangle\rangle} - \frac{\langle\langle \mathbf{z}, \mathbf{w} \rangle\rangle \langle\langle \mathbf{w}, \mathbf{z} \rangle\rangle \mathbf{y}}{\langle\langle \mathbf{z}, \mathbf{z} \rangle\rangle^2 \langle\langle \mathbf{w}, \mathbf{w} \rangle\rangle} \right), \quad (23)$$

Since the embedding \mathbf{z} should be constrained within the unit ball model, we apply the same projection strategy as [29] via a small constant ε :

$$\operatorname{proj}(\mathbf{z}) = \mathbf{z} / (|\mathbf{z}| - \varepsilon), \text{ if } |\mathbf{z}| \geq 1, \text{ else } \mathbf{z}. \quad (24)$$

To sum up, the update of \mathbf{z} at the t -th iteration is

$$\mathbf{z}^{(t)} \leftarrow \operatorname{proj}(\mathbf{z}^{(t-1)} - \eta^{(t)} \nabla_{\mathbf{R}} L(\mathbf{z})) = \operatorname{proj}(\mathbf{z}^{(t-1)} - \eta^{(t)} \frac{1}{ds^2} \nabla_{\mathbf{E}} L(\mathbf{z})). \quad (25)$$

The RSGD steps of the unit ball embeddings are presented in Algorithm 1.

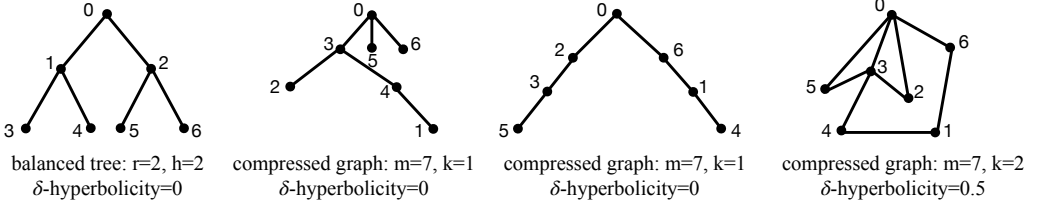


Fig. 1. Simple examples of the synthetic data. The numbers $\{0, 1, \dots, 6\}$ represent the nodes. The compressed graph- $(m = 7, k = 2)$ on the right are aggregated from the middle two compressed graphs- $(m = 7, k = 1)$.

5 EXPERIMENTS

In experiments, we evaluate the performances of our approach and baselines on various hierarchical structures, including synthetic graphs and real-world data. We focus on the graph reconstruction task and the link prediction task.

5.1 Experimental Settings

5.1.1 Data. We use synthetic and real-world data that exhibit underlying hierarchical structures to evaluate our approach. The details are given in the following.

Synthetic. We generate various balanced trees and compressed graphs using NetworkX package [22].⁴ For **balanced trees**, we generate the balanced tree with degree r and depth h . For **compressed graphs**, we generate k random trees on m nodes and then aggregate their edges to form a graph. We give some examples of the synthetic data in Figure 1. As we can see, the compressed graphs- $(m = 7, k = 1)$ are random trees on 7 nodes, so their δ -hyperbolicities are 0. The compressed graph- $(m = 7, k = 2)$ is no longer a tree after aggregating from two trees. Its local structures are more varying and complicated.

ICD10. The 10-th revision of International Statistical Classification of Diseases and Related Health Problems (ICD10) [6] is a medical classification list provided by the World Health Organization.⁵ We construct its full transitive closure as the ICD10 dataset.

YAGO3-wikiObjects. YAGO3 [26] is a huge semantic knowledge base.⁶ It provides a taxonomy derived from Wikipedia and WordNet. We extract the Wikipedia concepts and entities that are descendants of $\langle wikicat_Objects \rangle$ as well as the hypernymy edges among them. We compute the transitive closure of the sampled taxonomy to construct the YAGO3-wikiObjects dataset.

WordNet-noun. WordNet [27] is a large lexical database.⁷ The hypernymy relation among all nouns forms a noun hierarchy. We use its full transitive closure as the WordNet-noun dataset.

Xiphophorus. The Xiphophorus is a multitree dataset from [10], which contains 160 trees representing mrbayes consensus trees inferred for different genomic regions on 26 Xiphophorus fishes. Some examples of its subtrees are in Figure 2 and its cloud tree plot is in Figure 5. We use the saved MultiTree object in toytree package.⁸

For the multitree (Xiphophorus), we use the full dataset as the training set and the edges containing the leaf nodes as the test set. For each real-world taxonomy (ICD10, YAGO3-wikiObjects,

⁴<https://networkx.org/documentation/stable/reference/generators.html>.

⁵<https://www.who.int/standards/classifications/classification-of-diseases>.

⁶<https://yago-knowledge.org/>.

⁷<https://wordnet.princeton.edu/>.

⁸<https://toytree.readthedocs.io/en/latest/7-multitrees.html>.

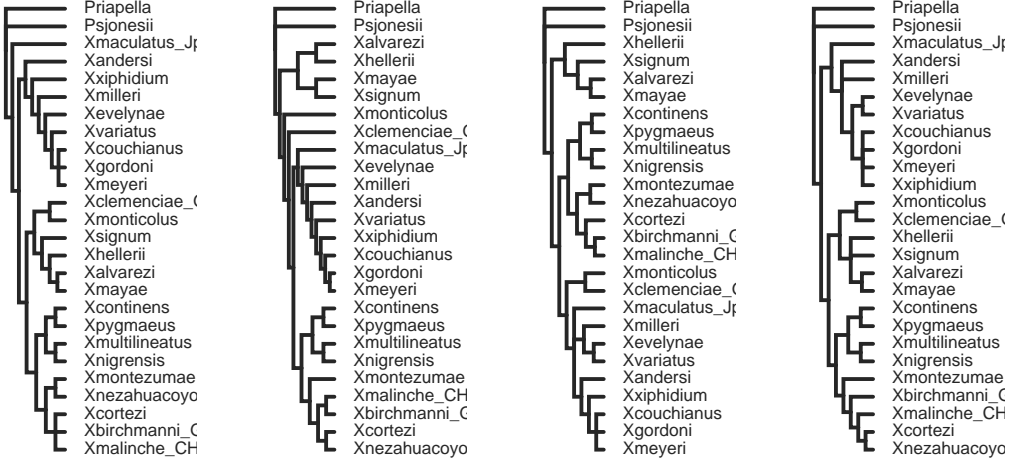


Fig. 2. Some subtrees of Xiphophorus. The multitree dataset Xiphophorus contains 160 trees on 26 Xiphophorus fishes as leaf nodes.

Table 2. The real-world datasets statistics.

	Xiphophorus	ICD10	YAGO3-wikiObjects	WordNet-noun
Nodes	3,562	19,155	17,375	82,115
Edges	7,536	78,357	153,643	743,086
Depth	13	6	16	20
Training edges	7,536	70,521	138,277	668,776
Valid/Test edges	4,160	3,918	7,683	37,155
δ -hyperbolicity	2.5	0.0	1.0	0.5

WordNet-noun), we randomly split the edges into train-validation-test sets with the ratio 90%:5%:5%. We make sure that any node in the validation and test sets must occur in the training set since otherwise, it cannot be predicted. But the edges in the validation and test sets do not occur in the training set since they are disjoint. We provide the statistics of the real-world datasets in Table 2. The Gromov’s δ -hyperbolicity [19] measures the tree-likeness of graphs (refer to Section 3.1.2 for definition). The lower δ corresponds to the more tree-like graph and trees have 0 δ -hyperbolicity.

5.1.2 Tasks. We evaluate the following two tasks:

Graph reconstruction: we train the embeddings of the full data and then reconstruct it from the embeddings. The task evaluates representation capacity.

Link prediction: we train the embeddings on the training set and predict the edges in the test set. The task evaluates generalization performance.

5.1.3 Baselines. We compare our approach **UnitBall** to the following methods: the state-of-the-art combinatorial construction-based hyperbolic embedding method **TreeRep** [38],⁹ the **Product** hyperbolic embeddings [20],¹⁰ the optimization-based hyperbolic embeddings in the **Poincaré** ball

⁹<https://github.com/rsonthal/TreeRep>.

¹⁰<https://github.com/HazyResearch/hyperbolics>.

model [29] and the **Hyperboloid** model [30], the simple **Euclidean** embedding model.¹¹ Note that Euclidean, Poincaré, Hyperboloid, and our approach UnitBall use the same loss function but learn in the different geometrical spaces. Therefore, the comparisons reveal the capacities of different geometrical models in different spaces.

For the baselines, we use their released codes to train the embeddings. For all methods, we tune the hyperparameters by grid search. For the graph reconstruction task, we tune the hyperparameters on balanced tree-(15,3) in 20-dimensional embedding spaces (10-dimensional complex hyperbolic space for UnitBall), while for the link prediction task, we tune the hyperparameters on the validation sets in 32-dimensional embedding spaces (16-dimensional complex hyperbolic space for UnitBall). In all experiments, we report the mean results over 5 running executions.

The n -d complex hyperbolic embeddings have around double parameters of the n -d real embeddings since the n -d complex hyperbolic vectors have n -d real part and n -d imaginary part. For a fair comparison, in each experimental setting, we compare our n -d complex hyperbolic embeddings of UnitBall against the $2n$ -d embeddings of the baselines. The results will also demonstrate that the n -d complex hyperbolic space is not simply the $2n$ -d hyperbolic space, they have different capacities.

5.1.4 Evaluation. Our evaluation closely follows the setting of [29, 30], which infers the hierarchies from distances in the embedding space. We use the mean average precision (**MAP**), mean reciprocal rank (**MRR**), and **Hits@N** as our evaluation metrics, which are widely used for evaluating ranking and link prediction. Specifically, for each test edge (z, w) , we compute the distance between the embeddings $d_{\mathcal{B}_{\mathbb{C}}^n}(z, w)$ and rank it among the distances of all unobserved edges for z : $\{d_{\mathcal{B}_{\mathbb{C}}^n}(z, w') : (z, w') \notin \text{Training}\}$. We then report the following evaluation metrics of the rankings. Denote E_{test} as the test edge set and $V = \{z | \exists w, (z, w) \in E_{test}\}$ as the test node set. Let $NE_z = \{w_1, w_2, \dots, w_{|NE_z|}\}$ be the ground truth neighbor set of node z .

Mean average precision (MAP). The average precision (AP) is a way to summarize the precision-recall curve into a single value representing the average of all precisions and the MAP score is calculated by taking the mean AP over all classes. For a node z , from the learned embeddings, we can obtain the nodes closest to its embedding z . Let R_{z, w_i} be the smallest set of such nodes that contains w_i (the i -th neighbor of z). Then the MAP is defined as:

$$\text{MAP} = \frac{1}{|V|} \sum_{z \in V} \frac{1}{|NE_z|} \sum_{w_i \in NE_z} \text{Precision}(R_{z, w_i}).$$

Mean reciprocal rank (MRR). The MRR is a statistic measure for evaluating a list of possible responses to a sample of queries, ordered by the probability of correctness. For a node z , from the learned embeddings, we can rank its distances with other nodes from the smallest to the largest. Let rank_{w_i} be the rank of w_i (the i -th neighbor of z). Then the MRR is defined as:

$$\text{MRR} = \frac{1}{|V|} \sum_{z \in V} \frac{1}{|NE_z|} \sum_{w_i \in NE_z} \frac{1}{\text{rank}_{w_i}}.$$

The proportion of correct types that rank no larger than N (Hits@N). Hits@N measures whether the top N predictions contain the ground truth labels. For a node z , from the learned embeddings, we can obtain the set of N nodes closest to its embedding z , denoted as R_z^N . Then the Hits@N is

¹¹<https://github.com/facebookresearch/poincare-embeddings>. The repository provides the implementation for Euclidean, Poincaré, and Hyperboloid.

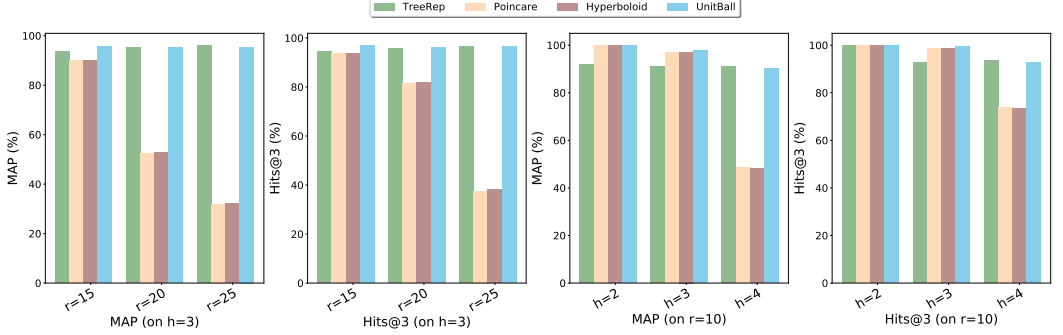


Fig. 3. Evaluation of graph reconstruction on synthetic balanced trees in 20-d embedding spaces (10-d complex hyperbolic space for UnitBall). r represents the degree while h represents the depth.

defined as:

$$\text{Hits@}N = \frac{1}{|V|} \sum_{z \in V} \mathbb{I}(|R_z^N \cap NE_z| \geq 1),$$

where $\mathbb{I}(|R_z^N \cap NE_z| \geq 1)$ is the indicator function.

5.1.5 Hardware. We conduct all the experiments except TreeRep on four NVIDIA GTX 1080Ti GPUs with 8GB memory each. For TreeRep, we need more memory to store the distance matrices, so we use a 96-core NVIDIA T4 GPU server with 503GB memory.

5.2 Experiments on Synthetic Data

5.2.1 Graph Reconstruction Results on Balanced Trees. To compare the representation capacities of UnitBall and the hyperbolic embedding models for the tree structures, we evaluate the graph reconstruction task on the synthetic balanced trees. A balanced tree- (r, h) has degree r and depth h , so it has $r^0 + \dots + r^h$ nodes and $r^0 + \dots + r^h - 1$ edges. The δ -hyperbolicity of any balanced tree is 0. We embed the balanced trees into 20-d hyperbolic space for the baselines and 10-d complex hyperbolic space for UnitBall.

Figure 3 presents the MAP and Hits@3 scores with varying r and h . We see that when the tree is in small scale, e.g., $(r, h) = (15, 3), (10, 2), (10, 3)$, all methods have very good performances, demonstrating the expected powerful capacities of hyperbolic geometry and complex hyperbolic geometry on tree structures. However, when the breadth or the depth increases, the performances of Poincaré and Hyperboloid drop rapidly, suggesting that the optimization-based embeddings in $\mathbb{H}_{\mathbb{R}}^{20}$ are not effective enough for reconstructing trees of such scales.

In comparison, UnitBall and TreeRep achieve stable performances for larger trees. TreeRep learns a tree structure from the data as an intermediate step and then embeds the learned trees into the hyperbolic space using Sarkar’s construction [34]. When the input data is a tree, TreeRep exactly recovers the original tree structure. Figure 3 shows that UnitBall achieves comparable or even better performances than TreeRep on the balanced trees. The results demonstrate that UnitBall does not compromise on trees. It produces high-quality embeddings for tree structures.

5.2.2 Graph Reconstruction Results on Compressed Graphs. To illustrate the benefits of UnitBall on varying hierarchical structures, we evaluate on the synthetic compressed graphs. The compressed graphs have local tree structures while being much more complicated than trees. Each compressed

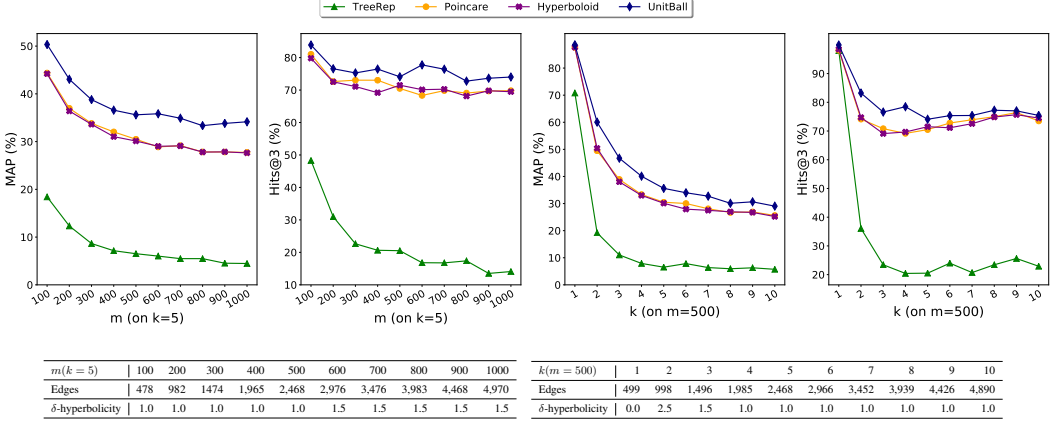


Fig. 4. Evaluation of graph reconstruction on synthetic compressed graphs in 20-d embedding spaces (10-d complex hyperbolic space for UnitBall). m represents the number of nodes in the graph while k represents the number of random trees aggregated to the graph (k controls the denseness and noise level of the graph). The statistics of the compressed graphs are provided in the tables.

graph- (m, k) consists of m nodes and is aggregated from k random trees on the m nodes. The bigger k corresponds to the denser and noisier graph.

Figure 4 depicts that the graph reconstruction results drop down with the increase of m and k , which represents the increase of graph scale and denseness respectively. Remarkably, UnitBall outperforms all baselines on the challenging data, showing that UnitBall handles the noisy locally tree-like structures better. TreeRep has comparable results with other methods when $(m, k) = (500, 1)$ since when $k = 1$, the graph is exactly a tree, i.e., $\delta = 0$. However, when $k > 1$ and $\delta > 0$, the data metrics deviate from tree metrics, in which case it does not help much to learn a tree structure from the data as an intermediate step.

As mentioned in Section 2, the product space embeddings [20] tackles the challenges in varying local structures by jointly learning the curvature and the embeddings of data in a product manifold. Although it is impractical to search for the best manifold combination among enormous combinations for each new structure, it is worth exploring the comparisons between the complex hyperbolic embeddings and products of hyperbolic embeddings. Therefore, we also evaluate the 16-dimensional UnitBall complex hyperbolic embeddings and 32-dimensional product hyperbolic embeddings on $(\mathbb{H}_{\mathbb{R}}^2)^{16}$, $(\mathbb{H}_{\mathbb{R}}^4)^8$, $(\mathbb{H}_{\mathbb{R}}^8)^4$. The results are reported in Table 3.

When $k = 1$ ($\delta = 0$), UnitBall and the product hyperbolic embeddings both have much better performances. When $k > 1$, UnitBall still outperforms the product hyperbolic embeddings by a large margin. Especially when $m = 500, k = 2, 3$, the δ is big, which means the graph deviates from tree structures a lot, the product hyperbolic embeddings fail to reconstruct the graph while UnitBall successfully handles the noisy structures.

5.3 Experiments on Real-World Data

5.3.1 Results on the Real-World Taxonomies. In this section, we evaluate the performances on the link prediction task for real-world taxonomies. Table 4 presents the results in 32-d embedding spaces for baselines and 16-d complex hyperbolic space for UnitBall. Predicting missing links requires generalization capacity, and UnitBall still has the best performances on all three datasets. Besides,

Table 3. Results of MAP and Hits@3 on graph reconstruction in synthetic compressed graphs. The best results are shown in boldface. The second best results are underlined.

	Compressed graph- (m, k) (MAP)									
k (m=500)	1	2	3	4	5	6	7	8	9	10
δ -hyperbolicity	0.0	2.5	1.5	1.0	1.0	1.0	1.0	1.0	1.0	1.0
Product- $(\mathbb{H}_{\mathbb{R}}^2)^{16}$	<u>66.06</u>	<u>7.60</u>	<u>7.55</u>	11.09	<u>20.81</u>	24.56	24.07	21.62	18.79	16.16
Product- $(\mathbb{H}_{\mathbb{R}}^4)^8$	65.77	7.14	7.24	<u>11.79</u>	20.60	<u>24.94</u>	22.85	<u>22.32</u>	18.50	16.27
Product- $(\mathbb{H}_{\mathbb{R}}^8)^4$	65.42	6.28	6.81	11.43	19.03	23.88	<u>24.99</u>	20.50	<u>18.99</u>	<u>16.45</u>
UnitBall- $\mathbb{H}_{\mathbb{C}}^{16}$	84.72	52.74	44.73	39.75	35.32	33.17	32.48	29.13	29.86	28.58
	Compressed graph- (m, k) (Hits@3)									
Product- $(\mathbb{H}_{\mathbb{R}}^2)^{16}$	<u>80.34</u>	8.14	9.84	14.81	<u>37.45</u>	45.97	47.89	<u>47.19</u>	<u>40.85</u>	38.88
Product- $(\mathbb{H}_{\mathbb{R}}^4)^8$	<u>80.34</u>	<u>8.35</u>	9.43	16.23	36.23	<u>47.98</u>	44.87	<u>47.19</u>	39.84	36.87
Product- $(\mathbb{H}_{\mathbb{R}}^8)^4$	79.36	6.21	<u>10.25</u>	<u>16.63</u>	31.38	44.15	<u>49.50</u>	43.57	40.64	<u>40.08</u>
UnitBall- $\mathbb{H}_{\mathbb{C}}^{16}$	97.71	75.87	72.61	74.92	73.21	73.12	76.12	76.57	75.72	74.08
	Compressed graph- (m, k) (MAP)									
m (k=5)	100	200	300	400	500	600	700	800	900	1000
δ -hyperbolicity	1.0	1.0	1.0	1.0	1.0	1.5	1.5	1.5	1.5	1.5
Product- $(\mathbb{H}_{\mathbb{R}}^2)^{16}$	30.53	<u>29.15</u>	<u>25.72</u>	21.74	<u>20.81</u>	<u>19.34</u>	19.07	16.63	<u>15.59</u>	<u>14.82</u>
Product- $(\mathbb{H}_{\mathbb{R}}^4)^8$	<u>32.03</u>	27.63	23.82	<u>22.32</u>	20.60	17.94	<u>19.12</u>	<u>17.36</u>	15.39	14.74
Product- $(\mathbb{H}_{\mathbb{R}}^8)^4$	31.39	27.95	23.17	19.90	19.03	17.96	18.09	16.13	13.86	13.47
UnitBall- $\mathbb{H}_{\mathbb{C}}^{16}$	47.80	40.93	38.52	35.81	35.32	35.68	34.73	34.69	34.92	34.88
	Compressed graph- (m, k) (Hits@3)									
Product- $(\mathbb{H}_{\mathbb{R}}^2)^{16}$	38.78	<u>52.02</u>	<u>43.58</u>	35.61	<u>37.45</u>	<u>34.29</u>	34.54	28.34	27.44	24.77
Product- $(\mathbb{H}_{\mathbb{R}}^4)^8$	46.94	43.43	39.53	<u>38.38</u>	36.23	29.58	<u>35.84</u>	29.35	<u>27.55</u>	<u>27.60</u>
Product- $(\mathbb{H}_{\mathbb{R}}^8)^4$	<u>54.08</u>	42.42	35.47	33.59	31.38	32.44	30.49	<u>29.72</u>	24.64	24.57
UnitBall- $\mathbb{H}_{\mathbb{C}}^{16}$	84.35	75.42	77.36	72.14	73.21	73.00	73.99	72.63	72.23	74.01

Table 4. Evaluation of taxonomy link prediction in 32-d embedding spaces (16-d complex hyperbolic space for UnitBall). The best results are shown in boldface. The second best results are underlined.

	ICD10			YAGO3-wikiObjects			WordNet-noun		
	MAP	MRR	Hits@3	MAP	MRR	Hits@3	MAP	MRR	Hits@3
Euclidean	3.75	3.72	2.39	4.85	4.45	2.78	5.59	5.36	3.16
TreeRep	4.96	7.92	8.49	20.19	21.85	27.19	9.30	9.98	11.90
Poincaré	<u>35.24</u>	<u>34.45</u>	52.71	30.06	28.47	41.61	25.46	23.99	<u>27.80</u>
Hyperboloid	34.80	34.01	<u>52.88</u>	<u>30.80</u>	<u>29.21</u>	<u>43.17</u>	<u>25.65</u>	<u>24.15</u>	27.50
UnitBall	47.88	46.96	70.28	33.33	31.85	47.41	27.29	25.93	32.95

we see that Euclidean shows shortages on these hierarchically-structured data, which is consistent with the results in previous works [29, 30]. Similar to the results on the graph reconstruction task, Poincaré and Hyperboloid have very close performances, while Hyperboloid has slightly better results. They have significant improvements over Euclidean, but they still fall behind UnitBall,

Table 5. Evaluation of graph reconstruction on the real-world taxonomies (the dimension is 32 for TreeRep and 16 for UnitBall). For memory cost, the unit is *GiB*.

	ICD10			YAGO3-wikiObjects			WordNet-noun		
	MRR	Hits@1	Memory	MRR	Hits@1	Memory	MRR	Hits@1	Memory
TreeRep	26.74	91.97	30	36.71	95.39	21	16.99	90.51	226
UnitBall	47.47	98.93	0.005	39.65	96.10	0.005	28.88	94.95	0.02

Table 6. Evaluation of taxonomy link prediction in different embedding dimensions (the embedding dimension for UnitBall is half of other models). The best results are shown in boldface. The second best results are underlined. TreeRep is not applicable to 128-d WordNet-noun due to the large memory cost, so we do not include the results.

	ICD10								
	8-dimensional			32-dimensional			128-dimensional		
	MAP	MRR	Hits@3	MAP	MRR	Hits@3	MAP	MRR	Hits@3
Euclidean	2.57	2.57	1.32	3.75	3.72	2.39	10.83	10.48	4.66
TreeRep	3.44	3.90	6.03	4.96	7.92	8.49	8.09	8.74	17.23
Poincaré	<u>35.73</u>	<u>34.94</u>	<u>53.10</u>	<u>35.24</u>	<u>34.45</u>	52.71	34.47	33.70	52.19
Hyperboloid	35.56	34.77	51.90	34.80	34.01	<u>52.88</u>	<u>34.93</u>	<u>34.15</u>	<u>52.98</u>
UnitBall	44.05	43.26	61.54	47.88	46.96	70.28	46.54	45.59	70.03
	YAGO3-wikiObjects								
	8-dimensional			32-dimensional			128-dimensional		
	MAP	MRR	Hits@3	MAP	MRR	Hits@3	MAP	MRR	Hits@3
Euclidean	1.02	0.92	0.57	4.85	4.45	2.78	16.67	15.76	15.97
TreeRep	16.91	17.48	27.53	20.19	21.85	27.19	21.18	23.44	32.84
Poincaré	29.70	28.13	41.64	30.06	28.47	41.61	29.93	28.35	41.53
Hyperboloid	<u>30.87</u>	<u>29.28</u>	<u>43.50</u>	<u>30.80</u>	<u>29.21</u>	<u>43.17</u>	<u>30.68</u>	<u>29.07</u>	<u>42.86</u>
UnitBall	31.40	29.98	44.25	33.33	31.85	47.41	32.76	31.28	46.25
	WordNet-noun								
	8-dimensional			32-dimensional			128-dimensional		
	MAP	MRR	Hits@3	MAP	MRR	Hits@3	MAP	MRR	Hits@3
Euclidean	1.07	1.05	0.63	5.59	5.36	3.16	14.33	13.35	8.82
Poincaré	<u>25.23</u>	<u>23.78</u>	27.63	25.46	23.99	<u>27.80</u>	25.33	23.86	27.41
Hyperboloid	25.73	24.24	<u>27.67</u>	<u>25.65</u>	<u>24.15</u>	27.50	<u>25.77</u>	<u>24.27</u>	<u>27.65</u>
UnitBall	24.91	23.76	30.27	27.29	25.93	32.95	27.29	25.91	32.77

which demonstrates our claims that the non-constant negative curvature of the complex hyperbolic space addresses the varying hierarchical structures on real-world taxonomies.

We notice that TreeRep does not perform well on the link prediction task. As mentioned in Section 2, the combinatorial construction-based embedding methods target minimizing the reconstruction distortion of data. However, minimizing the reconstruction distortion may overfit the training set, thus resulting in the unpromising generalization performance for unobserved edges. Hence, they are more suitable to learn the representation of graph data without missing links, such as the graph reconstruction tasks in Section 5.2. Therefore, here we compare UnitBall with TreeRep on the real-world taxonomy reconstruction task. The results are presented in Table 5. Its performance

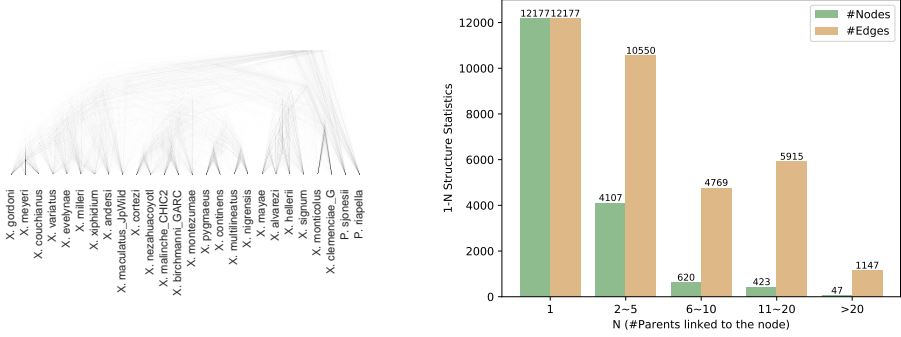


Fig. 5. **Left:** The cloud tree plot of Xiphophorus. **Right:** The 1- N structure statistics in YAGO3-wikiObjects *original* taxonomy. The horizontal axis represents the number of parents linked to a node. The vertical axis counts the number of nodes and edges in the 1- N structures. For example, there are 4, 107 nodes that link to N parents for $2 \leq N \leq 5$, and these links count to 10, 550 edges.

is much better than that on the link prediction task. In addition, UnitBall still outperforms TreeRep on reconstructing real-world taxonomies.

We also notice the memory issues of the combinatorial construction-based embedding methods. Although TreeRep is very efficient in embedding tree structures since it does not need the gradient-based optimization steps, it costs more memory resources for constructing the tree structures from data. It is basically a computation time vs. memory cost trade-off issue. For a graph with m nodes, TreeRep needs to construct a matrix of size $c \cdot m \times c \cdot m$ to construct the tree structure, where $1 \leq c \leq 2$ is a hyperparameter. We report the memory cost (GiB) in Table 5. UnitBall costs much less memory to learn the embeddings.

5.3.2 Exploring the Embedding Dimensions. In this section, we explore the link prediction performances in different embedding dimensions. The results are presented in Table 6. We find that with the increase of the embedding dimension, Euclidean can have big improvements, but its performances in 128-d still cannot surpass other methods in 8-d. TreeRep also achieves better results with the increase of dimension, but overall its performances on the link prediction task are not very promising. By comparison, Poincaré, Hyperboloid, and UnitBall achieve great results steadily. 8-d is already enough for Poincaré and Hyperboloid to handle the link prediction task while UnitBall has small improvements from 4-d to 16-d, then converges to the stable performance. Although on WordNet-noun, UnitBall in 4-d has slightly lower MAP and MRR than Poincaré and Hyperboloid in 8-d, it has much higher Hits@3.

5.3.3 Exploring 1- N Structure. A noteworthy difference between the real-world taxonomies and the tree structures is that the taxonomies contain many 1- N (1 child links to multiple parents) cases while in a tree each node except the root is linked to only 1 parent node. To investigate the advantages of complex hyperbolic geometry on the 1- N structures, we evaluate the performances of UnitBall, Poincaré, and Hyperboloid on predicting the 1- N edges. We evaluate on YAGO3-wikiObjects since it contains abundant 1- N structures. The statistics of the 1- N structures in YAGO3-wikiObjects *original* taxonomy (*original* means without computing the transitive closure) are given in Figure 5.

In this experiment, we train the embeddings on the full transitive closure of YAGO3-wikiObjects and then predict the 1- N edges. The results are reported on Table 7 and 8. We can see that UnitBall

Table 7. Results of Hits@1 and Hits@10 on predicting 1- N edges in YAGO3-wikiObjects. The embedding dimension is 16 for UnitBall while 32 for other models. The best results are shown in boldface.

N for 1- N edges	YAGO3-wikiObjects (Hits@1)					
	1	2 ~ 5	6 ~ 10	11 ~ 20	> 20	> 1
Poincaré	36.94	12.13	0.97	0.87	0.00	9.83
Hyperboloid	38.24	12.20	0.97	0.95	0.00	6.95
UnitBall	37.64	28.63	18.98	11.82	17.73	26.02
N for 1- N edges	YAGO3-wikiObjects (Hits@10)					
	1	2 ~ 5	6 ~ 10	11 ~ 20	> 20	> 1
Poincaré	93.10	65.48	60.11	49.09	43.97	63.29
Hyperboloid	92.80	65.51	63.49	51.93	45.39	63.95
UnitBall	92.42	76.35	65.91	66.19	70.21	74.03

Table 8. Results of MAP on **predicting 1- N edges in YAGO3-wikiObjects** and **reconstructing the leaf node links in Xiphophorus**. The embedding dimension is 16 for UnitBall and 32 for other models. The best results are shown in boldface.

N for 1- N edges	YAGO3-wikiObjects (MAP)						Xiphophorus (MAP)
	1	2 ~ 5	6 ~ 10	11 ~ 20	> 20	> 1	Leaf Links Reconstruction
Poincaré	60.73	16.87	9.28	9.31	9.46	15.29	89.75
Hyperboloid	61.49	15.01	9.25	9.50	9.54	13.80	89.80
UnitBall	58.41	26.73	13.28	10.17	11.64	23.61	91.95

has a very small compromise for the 1-1 edges, i.e., the edge pattern of tree structures. Nevertheless, UnitBall outperforms the hyperbolic models largely on 1- N structures for $N > 1$. Furthermore, Unitball has considerably huge improvement for $N > 6$, where the hyperbolic embedding models fail to make accurate predictions. Even for nodes that link to more than 20 parents, UnitBall can have accurate top 10 predictions for these edges. The results demonstrate that the complex hyperbolic embeddings maintain the advantages in the edge pattern of tree structures as well as handling more complicated hierarchical structures compared with the real hyperbolic embeddings.

5.3.4 Reconstruction Results on Multitree Structure. In combinatorics and order-theoretic mathematics, a multitree structure is a directed acyclic graph (DAG) in which the set of vertices reachable from any vertex induces a tree, or a partially ordered set (poset) that does not have four items a , b , c , and d forming a diamond suborder with $a \leq b \leq d$ and $a \leq c \leq d$ but with b and c incomparable to each other (also called a diamond-free poset [18]).¹² Obviously, the multitree structure is not a tree since one child node can have multiple parents in multitree. Note that the multitree structure is also different with 1- N structure since the multitree has more strict conditions, that is, the multitree is a diamond-free poset. By comparison, the 1- N structure is more general in taxonomies. For example, the subgraph of YAGO3-wikiObjects $\{(Nei\ Gaiman, is-a, British\ screenwriters), (Neil\ Gaiman, is-a, British\ fantasy\ writers), (British\ screenwriters, is-a, British\ writers), (British\ fantasy\ writers, is-a, British\ writers)\}$ is a 1- N structure, but it is not a multitree structure, because *British screenwriters* and *British fantasy writers* are incomparable to each other, i.e., there is no partial order between them.

¹²Here \leq denotes the partial order defined in the graph, e.g., the hypernymy relation.

Table 9. Evaluation of taxonomy link prediction on YAGO3-wikiObjects (the dimension is 32 for AttH and 16 for UnitBall).

	MAP	MRR	Hits@1	Hits@3
AttH	30.22	28.47	9.10	43.83
UnitBall	33.33	31.85	15.62	47.41

Table 10. Evaluation on link prediction task of GIL paper in ROC AUC (the dimension is 8 for UnitBall and 16 for HGCN and GIL).

	Disease	Airport	Pubmed	Citeseer	Cora
HGCN	90.80	96.43	95.13	96.63	93.81
GIL	99.90	98.77	95.49	99.85	98.28
UnitBall	99.09	96.61	98.80	99.34	97.64

Recall that our synthetic compressed graph is also aggregated from multiple trees, but it is not the multitree either. A compressed graph is aggregated from multiple random trees on the same set of nodes while the trees in a multitree structure share the same leaf nodes. Multitrees are widely used to represent multiple overlapping taxonomies over the same ground set.

In this section, we compare the performances of the hyperbolic models and UnitBall on Xiphophorus. Xiphophorus is a multitree dataset that is formed of 160 mrbayes consensus trees on 26 Xiphophorus fishes. Its cloud tree plot is in Figure 5. We reconstruct the edges containing the leaf nodes on Xiphophorus since the leaf links have the practical taxonomic meaning. The results are reported in the last column of Table 8. The results show that the complex hyperbolic geometry has a stronger ability to represent the multitree structure.

5.4 Comparison with Trainable Curvature Models

Since our work focuses on the representation of single-relation graphs, we do not evaluate the multi-relational knowledge graph embedding models or the neural networks in our main experiments. Nevertheless, to address the concerns of comparison with the trainable curvature models, we compare UnitBall with the hyperbolic knowledge graph embedding method AttH [7] and hyperbolic graph neural networks [8, 45].

5.4.1 Comparison with Hyperbolic Knowledge Graph Embeddings. In this section we evaluate AttH [7] on the single-relation taxonomy link prediction task. We use the released code and tune the hyperparameters on the validation set.¹³ From the results in Table 9, we see that UnitBall outperforms AttH in the single hypernymy relation link prediction task. However, UnitBall cannot infer multiple relations like AttH for now. We believe the future work of the complex hyperbolic embeddings will have promising improvements on multi-relational graph embeddings.

5.4.2 Comparison with Hyperbolic GNNs. Although hyperbolic GNNs also involve graph embeddings and can deal with the link prediction task, they make use of not only the edges between nodes but also the node features. The message propagation and attention mechanism make GNNs more flexible to handle various downstream tasks than shallow embeddings. In this section, we evaluate UnitBall on the link prediction task on the datasets of GIL [45]. The results of HGCN [8] and GIL [45]

¹³<https://github.com/HazyResearch/KGEmb>.

are copied from Table 2 of the GIL’s original paper [45]. We strictly follow their experimental settings and report the mean results of UnitBall in ROC AUC over 5 running executions.

The results are shown in Table 10. We can see that UnitBall outperforms HGCN on the five datasets. GIL is slightly better than UnitBall on most datasets while being outperformed by UnitBall on Pubmed. The results are very promising for UnitBall since UnitBall is a shallow embedding approach without deep architecture or feature interaction. We believe the complex hyperbolic embeddings will help to improve the GNNs and bring more insights into geometric deep learning.

6 CONCLUSION AND FUTURE WORK

In this paper, we present a novel approach for learning the embeddings of hierarchical structures in the unit ball model of the complex hyperbolic space. We characterize the geometrical properties of the complex hyperbolic space and formulate the embedding algorithm in the unit ball model. We exemplify the superiority of our approach over the graph reconstruction task and the link prediction task on both synthetic and real-world data, which cover the various hierarchical structures and two specific structures, namely multitree structure and 1- N structure. The empirical results show that our approach outperforms the hyperbolic embedding methods in terms of representation capacity and generalization performance. Motivated by our theoretical grounding and empirical success, we believe the complex hyperbolic embeddings will have promising improvements on the knowledge graph embeddings, neural networks, and other related applications.

REFERENCES

- [1] Ivana Balazevic, Carl Allen, and Timothy M. Hospedales. 2019. Multi-relational Poincaré Graph Embeddings. In *NeurIPS*. 4465–4475.
- [2] Alan F Beardon. 2012. *The geometry of discrete groups*. Vol. 91. Springer Science & Business Media.
- [3] Gary Bécigneul and Octavian-Eugen Ganea. 2019. Riemannian Adaptive Optimization Methods. In *ICLR (Poster)*. OpenReview.net.
- [4] Silvere Bonnabel. 2013. Stochastic Gradient Descent on Riemannian Manifolds. *IEEE Trans. Autom. Control* 58, 9 (2013), 2217–2229.
- [5] Antoine Bordes, Nicolas Usunier, Alberto García-Durán, Jason Weston, and Oksana Yakhnenko. 2013. Translating Embeddings for Modeling Multi-relational Data. In *NIPS*. 2787–2795.
- [6] Gerlind R Brämer. 1988. International statistical classification of diseases and related health problems. Tenth revision. *World health statistics quarterly. Rapport trimestriel de statistiques sanitaires mondiales* 41, 1 (1988), 32–36.
- [7] Ines Chami, Adva Wolf, Da-Cheng Juan, Frederic Sala, Sujith Ravi, and Christopher Ré. 2020. Low-Dimensional Hyperbolic Knowledge Graph Embeddings. In *ACL*. Association for Computational Linguistics, 6901–6914.
- [8] Ines Chami, Zhitao Ying, Christopher Ré, and Jure Leskovec. 2019. Hyperbolic Graph Convolutional Neural Networks. In *NeurIPS*. 4869–4880.
- [9] Hyunghoon Cho, Benjamin Demeo, Jian Peng, and Bonnie Berger. 2019. Large-Margin Classification in Hyperbolic Space. In *AISTATS (Proceedings of Machine Learning Research, Vol. 89)*. PMLR, 1832–1840.
- [10] R Cui, M Schumer, K Kruesi, RB Walter, P Andolfatto, and GG Rosenthal. 2013. Data from: phylogenomics reveals extensive reticulate evolution in Xiphophorus fishes. *Dryad Data Repository* (2013).
- [11] Jindou Dai, Yuwei Wu, Zhi Gao, and Yunde Jia. 2021. A Hyperbolic-to-Hyperbolic Graph Convolutional Network. In *CVPR*.
- [12] Shuyang Dai, Zhe Gan, Yu Cheng, Chenyang Tao, Lawrence Carin, and Jingjing Liu. 2021. APo-VAE: Text Generation in Hyperbolic Space. In *NAACL-HLT*. Association for Computational Linguistics, 416–431.
- [13] Nate Fisher. 2020. NOTES ON CURVATURE IN COMPLEX HYPERBOLIC SPACE. (2020). <https://sites.tufts.edu/natefisher/files/2020/11/Write-up.pdf>
- [14] Ruiji Fu, Jiang Guo, Bing Qin, Wanxiang Che, Haifeng Wang, and Ting Liu. 2014. Learning Semantic Hierarchies via Word Embeddings. In *ACL (1)*. The Association for Computer Linguistics, 1199–1209.
- [15] Octavian-Eugen Ganea, Gary Bécigneul, and Thomas Hofmann. 2018. Hyperbolic Entailment Cones for Learning Hierarchical Embeddings. In *ICML (Proceedings of Machine Learning Research, Vol. 80)*. PMLR, 1632–1641.
- [16] Octavian-Eugen Ganea, Gary Bécigneul, and Thomas Hofmann. 2018. Hyperbolic Neural Networks. In *NeurIPS*. 5350–5360.
- [17] William Mark Goldman. 1999. *Complex hyperbolic geometry*. Oxford University Press.

- [18] Jerrold R. Griggs, Wei-Tian Li, and Linyuan Lu. 2012. Diamond-free families. *J. Comb. Theory, Ser. A* 119, 2 (2012), 310–322.
- [19] Mikhael Gromov. 1987. Hyperbolic groups. In *Essays in group theory*. Springer, 75–263.
- [20] Albert Gu, Frederic Sala, Beliz Gunel, and Christopher Ré. 2019. Learning Mixed-Curvature Representations in Product Spaces. In *ICLR (Poster)*. OpenReview.net.
- [21] Çağlar Gülçehre, Misha Denil, Mateusz Malinowski, Ali Razavi, Razvan Pascanu, Karl Moritz Hermann, Peter W. Battaglia, Victor Bapst, David Raposo, Adam Santoro, and Nando de Freitas. 2019. Hyperbolic Attention Networks. In *ICLR (Poster)*. OpenReview.net.
- [22] Aric A. Hagberg, Daniel A. Schult, and Pieter J. Swart. 2008. Exploring Network Structure, Dynamics, and Function using NetworkX. In *Proceedings of the 7th Python in Science Conference*, Gaël Varoquaux, Travis Vaught, and Jarrod Millman (Eds.). Pasadena, CA USA, 11 – 15.
- [23] Shoshichi Kobayashi and Katsumi Nomizu. 1963. *Foundations of differential geometry*. Vol. 1. New York, London.
- [24] Dmitri Krioukov, Fragkiskos Papadopoulos, Maksim Kitsak, Amin Vahdat, and Marián Boguñá. 2010. Hyperbolic geometry of complex networks. *Phys. Rev. E* 82 (Sep 2010), 036106. Issue 3. <https://doi.org/10.1103/PhysRevE.82.036106>
- [25] Qi Liu, Maximilian Nickel, and Douwe Kiela. 2019. Hyperbolic Graph Neural Networks. In *NeurIPS*. 8228–8239.
- [26] Farzaneh Mahdizoltani, Joanna Biega, and Fabian M. Suchanek. 2015. YAGO3: A Knowledge Base from Multilingual Wikipedias. In *CIDR*. www.cidrdb.org.
- [27] George A. Miller. 1995. WordNet: A Lexical Database for English. *Commun. ACM* 38, 11 (1995), 39–41.
- [28] Ngaiming Mok. 1989. *Metric rigidity theorems on Hermitian locally symmetric manifolds*. Vol. 6. World Scientific.
- [29] Maximilian Nickel and Douwe Kiela. 2017. Poincaré Embeddings for Learning Hierarchical Representations. In *NIPS*. 6338–6347.
- [30] Maximilian Nickel and Douwe Kiela. 2018. Learning Continuous Hierarchies in the Lorentz Model of Hyperbolic Geometry. In *ICML (Proceedings of Machine Learning Research, Vol. 80)*. PMLR, 3776–3785.
- [31] Maximilian Nickel, Volker Tresp, and Hans-Peter Kriegel. 2011. A Three-Way Model for Collective Learning on Multi-Relational Data. In *ICML*. Omnipress, 809–816.
- [32] John G Ratcliffe, S Axler, and KA Ribet. 1994. *Foundations of hyperbolic manifolds*. Vol. 149. Springer.
- [33] Frederic Sala, Christopher De Sa, Albert Gu, and Christopher Ré. 2018. Representation Tradeoffs for Hyperbolic Embeddings. In *ICML (Proceedings of Machine Learning Research, Vol. 80)*. PMLR, 4457–4466.
- [34] Rik Sarkar. 2011. Low Distortion Delaunay Embedding of Trees in Hyperbolic Plane. In *Graph Drawing (Lecture Notes in Computer Science, Vol. 7034)*. Springer, 355–366.
- [35] Ryohei Shimizu, Yusuke Mukuta, and Tatsuya Harada. 2021. Hyperbolic Neural Networks++. In *ICLR (Poster)*.
- [36] Vered Shwartz, Yoav Goldberg, and Ido Dagan. 2016. Improving Hypernymy Detection with an Integrated Path-based and Distributional Method. In *ACL (1)*. The Association for Computer Linguistics.
- [37] Ondrej Skopek, Octavian-Eugen Ganea, and Gary Bécigneul. 2020. Mixed-curvature Variational Autoencoders. In *ICLR*. OpenReview.net.
- [38] Rishi Sonthalia and Anna C. Gilbert. 2020. Tree! I am no Tree! I am a low dimensional Hyperbolic Embedding. In *NeurIPS*.
- [39] Fabian M. Suchanek, Gjergji Kasneci, and Gerhard Weikum. 2007. Yago: a core of semantic knowledge. In *WWW*. ACM, 697–706.
- [40] Zequn Sun, Muhao Chen, Wei Hu, Chengming Wang, Jian Dai, and Wei Zhang. 2020. Knowledge Association with Hyperbolic Knowledge Graph Embeddings. In *EMNLP (1)*. Association for Computational Linguistics, 5704–5716.
- [41] Zhiqing Sun, Zhi-Hong Deng, Jian-Yun Nie, and Jian Tang. 2019. RotatE: Knowledge Graph Embedding by Relational Rotation in Complex Space. In *ICLR (Poster)*. OpenReview.net.
- [42] Théo Trouillon, Johannes Welbl, Sebastian Riedel, Éric Gaussier, and Guillaume Bouchard. 2016. Complex Embeddings for Simple Link Prediction. In *ICML (JMLR Workshop and Conference Proceedings, Vol. 48)*. JMLR.org, 2071–2080.
- [43] Wilhelm Wirtinger. 1927. Zur formalen theorie der funktionen von mehr komplexen veränderlichen. *Math. Ann.* 97, 1 (1927), 357–375.
- [44] Bishan Yang, Wen-tau Yih, Xiaodong He, Jianfeng Gao, and Li Deng. 2015. Embedding Entities and Relations for Learning and Inference in Knowledge Bases. In *ICLR (Poster)*.
- [45] Shichao Zhu, Shirui Pan, Chuan Zhou, Jia Wu, Yanan Cao, and Bin Wang. 2020. Graph Geometry Interaction Learning. In *NeurIPS*.